
Article:
Arif, E, Wang, C, Swiderska-Syn, MK et al. (9 more authors) (2021) Targeting Myosin 1c Inhibits Murine Hepatic Fibrogenesis. American Journal of Physiology: Gastrointestinal and Liver Physiology. ISSN 0193-1857

https://doi.org/10.1152/ajpgi.00105.2021

Targeting Myosin 1c Inhibits Murine Hepatic Fibrogenesis

Ehtesham Arif[1, 2], Cindy Wang[2], Marzena K Swiderska-Syn[3], Ashish K. Solanki[1], Bushra Rahman[1], Paul P. Manka[2,4], Jason D. Coombes[5,6], Ali Canbay[4], Salvatore Papa[7], Deepak Nihalani[1,8], Joshua H. Lipschutz[1,9], Wing-Kin Syn[2,10,11]*

[1]Department of Medicine, Nephrology Division, Medical University of South Carolina, Charleston, South Carolina, USA.
[2]Division of Gastroenterology & Hepatology, Medical University of South Carolina, Charleston, South Carolina, USA.
3Department of Pediatrics, Darby Children's Research Institute, Hollings Cancer Center, Medical University of South Carolina, Charleston, South Carolina, USA.
[4] Department of Medicine, University Hospital Knappschaftskrankenhaus, Ruhr-University Bochum, Germany.
[5] Institute of Hepatology, Foundation for Liver Research, London, UK
[6] School of Immunology and Microbial Sciences, Faculty of Life Sciences and Medicine, King's College London UK
[7] Leeds Institute of Medical Research at St. James's, Faculty of Medicine and Health, University of Leeds
[8] Division of Kidney, Urologic and Hematologic Diseases, National Institutes of Health, Bethesda, MD, USA
[9] Section of Nephrology, Ralph H Johnson Veterans Affairs Medical Center, Charleston, SC, USA
[10] Section of Gastroenterology, Ralph H Johnson Veterans Affairs Medical Center, Charleston, SC, USA
[11] Department of Physiology, Faculty of Medicine and Nursing, University of the Basque Country, UPV/EHU, Leioa, Spain

*Corresponding author
Wing-Kin Syn, M.D., Ph.D.
Professor of Medicine
Department of Gastroenterology & Hepatology
Medical University of South Carolina
Charleston, SC 29425
E-mail: synw@musc.edu
Phone: (843) 792-3267

Running Title: Myo1c and hepatic fibrogenesis

Keywords: Hepatic fibrosis**,** TGF-β signaling, Myo1c

Sources of support: This study is supported by the Division of Gastroenterology and Hepatology, MUSC (W.K.S), the Ralph H Johnson Veterans Affairs Medical Center (W.K.S), and National Institutes of Health, NIDDK, Grant RO3 5R03TR003038-02 (E.A.).

Word count:

ABSTRACT

Myosin 1c (Myo1c) is an unconventional myosin that modulates signaling pathways involved in tissue injury and repair. In this study, we observed that Myo1c expression is significantly upregulated in human chronic liver disease such as nonalcoholic steatohepatitis (NASH) and in animal models of liver fibrosis. High throughput data from the GEO-database identified similar Myo1c upregulation in mice and human liver fibrosis. Notably, TGF-β stimulation to hepatic stellate cells (HSCs, the liver pericyte and key cell type responsible for the deposition of extracellular matrix upregulates Myo1c expression, while genetic depletion or pharmacological inhibition of Myo1c blunted TGF-β induced fibrogenic responses, resulting in repression of α-SMA and Col1α1 mRNA. Myo1c deletion also decreased fibrogenic processes such as cell proliferation, wound healing response and contractility when compared with vehicle treated HSCs. Importantly, phosphorylation of SMAD2 and SMAD3 were significantly blunted upon Myo1c inhibition in GRX cells as well as Myo1c-KO MEFs upon TGF-β stimulation. Using the genetic Myo1c knockout (Myo1c-KO) mice, we confirmed that Myo1c is critical for fibrogenesis as Myo1c-KO mice were resistant to CCl4 induced liver fibrosis. Histological and immunostaining analysis of liver sections showed that deposition of collagen fibers and α-SMA expression were significantly reduced in Myo1c-KO mice upon liver injury. Collectively, these results demonstrate that Myo1c-mediates hepatic fibrogenesis by modulating TGF-β signaling and suggest that inhibiting this process may have clinical application in treating liver fibrosis.

INTRODUCTION

Chronic liver injury triggers a repair response that leads to liver fibrosis (i.e., liver scarring), which is characterized by the excessive accumulation of collagenous extracellular matrices (ECMs). This repair response occurs as a result of various insults including toxins, autoimmune disorders, cholestatic or metabolic diseases or viral infections, and leads to the development of fibrosis, cirrhosis, and cirrhosis-associated complications such as portal hypertension, hepatocellular carcinoma, and liver failure (1-3). Hepatic stellate cells (HSCs) are the liver pericytes which are considered the principal source of extracellular matrix proteins including collagen in the liver. Complex molecular mechanisms and signaling pathways play critical roles in the fibrogenic process and transforming growth factor-β1 (TGF-β1) is a prototypical profibrogenic cytokine which activates HSC and promotes collagen deposition (4). Intracellular signal transducers Smads whose phosphorylation and subsequent translocation into the nucleus upon TGF-β1 activation regulate expression of profibrotic target genes that contributes to collagen synthesis and liver fibrosis (5, 6).

Myo1c is an unconventional class I myosin and an actin-based molecular motor, which is actively involved in various cellular functions including intracellular trafficking, cell adhesion, motility and maintenance of membrane tension (7-10). Myo1c is expressed in various cell types and is generally associated with actin-rich cortical membrane structures such as filopodia, lamellipodia, and ruffles (11). The *Myo1c* gene has two isoforms, which are referred to as cytoplasmic (cMYO1C) and nuclear Myo1c (NM1) (12). NM1 differs from cMYO1C by the presence of 16 or 35 additional amino acids at the N-terminus. While

the cMYO1C interacts with various proteins and participates in cellular functions, NM1 is involved in chromatin remodeling, transcription, mRNA maturation, and chromosome movement (12-14). Our previous study showed that NM1 targets TGF-β responsive gene GDF-15 that contributes to the fibrogenic process in podocytes (10). Various cellular and signaling functions were also observed that confirmed the role of cMYO1C in fibrosis. Notably, another study showed that the Myo1c inhibitor Pentachloropseudilin (PCIP) inhibited TGF-β activity by accelerating TGF-β receptor turnover. PCIP attenuated TGF-β-induced smad2/3 phosphorylation and repressed expression of vimentin, N-cadherin, and fibronectin and, thus, blocking TGF-β-induced epithelial to mesenchymal transition (EMT) (7). Since TGF-β-signaling plays a major role in hepatic fibrogenesis, we evaluated the pathophysiological significance of Myo1c in hepatic fibrogenesis using *in-vitro* and *in-vivo* models.

RESULTS

***Myo1c* expression was significantly increased with hepatic fibrosis**: The first evidence for the involvement of Myo1c in hepatic fibrosis came from high throughput data. We first examined the gene expression omnibus (GEO) database (GEO # GDS3087) (15), where microarray and next generation analysis were performed in livers of animals lacking Trim24 (a ligand-dependent nuclear receptor transcriptional co-regulator) and control liver tissue, where the loss of Trim24 was associated with the development of liver fibrosis and HCC (15, 16). We found that Myo1c expression was significantly upregulated in liver tissues with fibrosis and HCC when compared with the normal liver **(Fig. 1A)**. In another throughput data (GEO # GSE49541) (17) which included patients with a full

spectrum of nonalcoholic fatty liver disease (NAFLD) severity, Myo1c expression was significantly higher among those with advanced NAFLD (fibrosis stage 3-4), compared with early NAFLD (fibrosis with stage 0-1) (**Fig. 1B**).

Further, Myo1c expression was analyzed through immunohistochemistry in representative liver tissues from humans and animal models of liver fibrosis. Myo1c expression was found to be significantly increased in human non-alcoholic steatohepatitis (NASH) fibrosis when compared with the healthy liver (**Fig. 1C-D**). In mice fed the methionine-choline deficient (MCD) diet (a well characterized model of NASH fibrosis) (18) and mice treated with carbon tetrachloride (CCl4) (another model of liver fibrosis) (19), Myo*1c* expression were also significantly upregulated, when compared to normal chow-fed or vehicle-treated animals, respectively (**Fig. 1E-H**). Increased Myo1c expression in CCl4 treated mice were further confirmed by western blot **(Supplemental Fig. 1A-B)**. Prolonged feeding with the high-fat-diet (HFD) also induces hepatic fibrogenesis (20), thus we also examined the expression of Myo1c in these tissues. We found that Myo1c mRNA was significantly increased in livers from mice fed the HFD, which mirrored α-SMA expression **(Supplemental Fig.1 C-D)**.

Since TGF-β signaling is a prototypical cytokine involved in tissue fibrogenesis, we next evaluated if TGF-β modulated expression of Myo1c. Treatment of the mouse hepatic stellate cells (HSC) line, GRX (21) significantly increased the *Myo1c* expression **(Fig. 1I-J)**. We also evaluated responses of mouse embryonic fibroblasts (MEFs) to TGF-β stimulation. Whilst MEFs are not tissue pericytes, they resemble fibroblasts in culture (22,

23), and were used as another model. We noted similar increases in Myo1c mRNA when mouse MEFs were treated with TGF-β (**Fig. 1I-J**).

Targeting Myo1c attenuated the fibrogenic response: Since TGF-β signaling is the primary driver of fibrogenesis (24) and we have shown that Myo1c is upregulated with liver fibrosis, we next evaluated if loss of *Myo1c* directly inhibits fibrogenesis. To this end, we infected GRX with Myo1c-specific short hairpin RNA (shMyo1c-GRX) (which knockdown Myo1c gene expression); we observed >90% repression of Myo1c mRNA (**Fig. 2A-B)**. Treatment with TGF-β significantly upregulates fibrogenic gene expression (α-SMA and Col1α1) in normal GRX cells, but these changes were significantly blunted in shMyo1c-GRX cells when compared with control (shScr-GRX) (i.e., GRX cells infected with scrambled short hairpin RNA) **(Fig. 2C-D)**. To confirm these findings, we repeated experiments using a pharmacologic approach. Pentachloropseudilin (PCIP) is a known Myo1c inhibitor, and the treatment of GRX cells with PCIP similarly, led to an attenuated fibrogenic response to TGF-β treatment **(Fig. 2E-F)**.

Dysregulation in cell proliferation and migration are associated with fibrogenesis (25, 26), and Myo1c has been reported to play key roles in cell motility, trafficking, cell migration and/or differentiation (8, 11, 27). shScr-GRX (control) and shMyo1c-GRX were analyzed for cell proliferation using the cell counting kit-8 (CCK-8) assay. We found that loss of Myo1c was associated with significantly reduced number of viable cells in shMyo1c-GRX **(Fig. 2G)**. Sulforhodamine B (SRB) based cell proliferation assay further confirmed the significant reduction in cell proliferation upon Myo1c knockdown **(Fig. 2H)**. Abnormal

wound healing results in tissue fibrosis (28, 29), and the scratch assay is widely used to evaluate the wound healing response(30). We found that wound healing was significantly inhibited in shMyo1c-GRX cells compared with control shScr-GRX **(Fig. 2I-J)**. Semi-quantitative analysis confirmed a significant reduction in cell migration distance (in μM) in shMyo1c-GRX cells: shScr-GRX (0.418μM) vs shMyo1c-GRX (0.254μM)**.** The collagen gel contraction (CGC) assay is another established method to study the fibrogenic response in presence of various stimuli including TGF-β (31, 32). It also provides information about the collagen remodeling in these cells (32). The effects of Myo1c loss on collagen gel contraction was performed in GRX cells either in presence of TGF-β or vehicle. TGF-β stimulation induced 54% of gel contraction in shScr-GRX (control) cells compared to 17% in shMyo1c-GRX **(Fig. 2K-L)**. Semi-quantitative analysis confirmed a significant reduction in TGF-β1 induced cell contraction upon Myo1c deletion.

To further validate our findings, we generated MEFs from 13.5 days embryos of Myo1c flox/flox mice. We treated these MEFs with either β-gal or Cre virus to generate control and Myo1c knockout MEFs, respectively. Whilst MEFs are not tissue pericytes, they resemble fibroblasts in culture (22, 23). We observed a significant loss of Myo1c protein in MEFs treated with the cre virus **(Fig. 3A)**. Control (*Myo1c$^{fl/fl}$-MEFs+βGal)* and Myo1c-KO (*Myo1c$^{fl/fl}$-MEFs+Cre)* MEFs were then treated with TGF-β and fibrogenic response analyzed through qPCR and immunofluorescence. qPCR analysis showed a significant upregulation of α-SMA and Col1α1 expression in control MEFs, but this was attenuated in Myo1c-KO MEFs **(Fig. 3B-C),** consistent with changes observed in shMyo1c-GRX cells **(Fig. 2C-D)**. Immunofluorescence imaging followed by quantitative analysis corroborated

our findings, where significant increases in α-SMA protein was detected in control MEFs, but not in Myo1c-KO MEFs **(Fig. 3D-E)**.

Loss of Myo1c attenuated TGF-β–signaling: We next evaluated if attenuation of fibrogenic responses observed with Myo1c inhibition (pharmacologic) and Myo1c deletion (genetic) were associated with the changes in downstream components of the TGF-β signaling pathway. GRX cells were treated with TGF-β or vehicles in presence or absence of PCIP, a pharmacological inhibitor of Myo1c (33). Western blotting analysis showed significant reduction in phosphorylation of SMAD2 and SMAD3 upon Myo1c inhibition in GRX cells. **(Fig. 4A-B).** Control or Myo1c-KO MEFs were similarly treated with TGF-β for 48 hours; at the end of treatment, cells were harvested, and western blot performed. We detected a comparable reduction in levels of phosphorylated SMAD2 and SMAD3 in Myo1c-KO MEFs **(Fig. 4C-D)**. These results in aggregate, confirm that loss Myo1c inhibits liver fibrogenesis.

Myo1c deletion attenuated CCl4 induced liver fibrosis: To understand the physiological significance of Myo1c, we used global Myo1c knockout mice as described in our previous work (10). In brief, Myo1c flox/flox mice were crossed with CMV cre mice obtained from the Jackson laboratory (B6.C-Tg(CMV-cre)1Cgn/J; Stock No: 006054). Cre recombination deletes the critical 5-13 exon of Myo1c as presented in **fig. 5A**. Deletion of Myo1c was confirmed through the western blotting analysis using specific Myo1c antibody **(Fig. 5B)**. Wild-type and Myo1c-KO mice were treated with either CCl4 (0.7ul/g body weight) or Vehicle (corn oil) and tissue were harvested at 5^{th} week (19, 34, 35).

Schematic figure of experimental design is presented in **fig. 5C.** At the end of study, livers were harvested and stained with Masson's trichrome and Sirius-red to assess the degree of fibrosis **(Fig. 5D-F)**. Loss of Myo1c resulted in significantly less liver fibrosis compared with control mice **(Fig. 5D)**. Semi-quantitative analysis of Masson's trichrome images showed 8.2 % of area with collagen deposition in control vs 3.37% in Myo1c-KO mice ($p<0.001$) **(Fig. 5E)**. Similar changes were seen with Sirius-red staining: 9.7 % of area with collagen deposition in control vs 5.7% in Myo1c-KO mice. **(Fig. 5G)**.

α-SMA is an actin isoform and a specific marker for HSC activation and fibrogenesis (36). Loss of Myo1c was associated with significantly fewer α-SMA positive cells by immunofluorescence and immunohistochemistry **(Fig. 6A-C).** Analysis of mean pixel intensity in fluorescence images and α-SMA positive area also confirmed the significant increase of α-SMA protein expression in CCl4-treated wild-type mice but this was significantly repressed in Myo1c-KO mice **(Fig. 6B-D)**. Collectively, these results showed that loss of Myo1c attenuated CCl4 induced liver fibrosis in mice.

DISCUSSION

The mechanisms of tissue fibrogenesis is complex and TGF-*β*1 dependent signaling is a prototypical pathway involved in liver fibrosis. In this study, we showed that the unconventional class I myosin and actin-based molecular motor is a key modulator of liver fibrosis. In a series of *in vitro* and *in vivo* studies, we showed that Myo1c is upregulated in liver fibrosis, where it enhanced canonical TGF-β signaling. Conversely, targeting

Myo1c pharmacologically or genetically significantly reduced levels of phosphorylated Smads and alleviated the liver repair response.

This novel role of Myo1c in tissue fibrogenesis simply recapitulates its function in cell adhesion, motility and maintenance of membrane tension (8, 9, 11). Interestingly, Myo1c is also highly expressed in adipocytes where it facilitates recycling of the glucose transporter (37); specifically, by regulating the trafficking of intracellular GLUT4-containing vesicles to the plasma membrane in response to insulin (37). This is relevant to fibrogenesis because recent data show that metabolic reprogramming can regulate HSC activation and fibrogenic responses (38). Myo1c also stabilizes actin and participates as an important mediator of VEGF-induced VEGFR2 delivery to the cell surface and plays a role in angiogenic signaling (39), a feature characteristic of liver fibrosis. These studies in aggregate, support the role for Myo1c in hepatic fibrogenesis, and is consistent with our previous study where we had shown that Myo1c regulates fibrogenesis in kidney podocytes (10), and another group had reported that treatment with PCIP repressed TGF-β-induced epithelial to mesenchymal transition (EMT) (7).

Although Myo1c appears to be a critical modulator of canonical TGF-β signaling, the mechanisms by which Myo1c effects changes in the levels of Smad phosphorylation is unclear, but is likely to involve both isoforms of the Myo1c protein. Studies to date suggest that the cytoplasmic isoform is involved in intracellular trafficking and the stabilization of key cellular proteins, while the nuclear isoform regulates chromatin remodeling and gene expression (8, 12, 14, 27, 37, 40). It is therefore, possible that Myo1c could regulate

adaptor proteins or surface expression of TGF-β receptors (similar to its regulation of VEGFR2 expression). As growth differentiation factor (GDF)15 is a downstream effector of Myo1c (10), and has recently been shown to directly activate lung fibroblasts and macrophages (41), future studies will be needed to determine if Myo1c-associated GDF15 secretion also contributes to the profibrogenic milieu in chronic liver disease. These latter studies are important because Myo1c is ubiquitously expressed and the generalized targeting of Myo1c would likely lead to adverse clinical outcomes; targeting downstream effectors such as GDF15, and/or in a tissue-/cell-selective manner would significantly mitigate side effects.

In conclusion, we showed for the first time that Myo1c plays an important role in regulating hepatic fibrogenesis, and that targeting Myo1c protects mice from liver fibrosis.

METHODS

Cell culture: The clonally-derived rat myofibroblastic hepatic stellate cell (HSCs/GRX) (21) were cultured in DMEM media supplemented with 10% FBS and 1% pen/strep as described earlier (42). Mouse embryonic fibroblasts (MEFs) were isolated from Myo1c-flox/flox mice using embryos at E13.5 from the pregnant females as described earlier (23). MEFs were also cultured in DMEM medial and supplemented with 10% FBS, 1% penicillin/streptomycin, and 1% Non-Essential Amino Acids. All these cells were plated on a 10 cm^2 dish and incubated at 37 °C in the presence of 5% CO2. The Myo1c inhibitor PCIP was used at a concentration of 1 μM (33). These cells were stimulated with TGF-β as described (10). Briefly, cells were incubated overnight in DEME medium with 0.1% FBS and stimulated with 5ng/ml of TGF-β in the same medium for a period of 48hours.

Generation of Myo1c-knockdown and knockout cells: Myo1c knockdown in GRX cells were generated using lentiviral vector carrying Myo1c shRNA (TRCN0000100742, Sigma) and control knockdown cells were generated using scramble lentiviral vector (SHC016V, Sigma). MEFs Myo1c-KO and control-KO cells were generated by transducing adenovirus either adeno-cre or adeno-β-gal virus for 24 hours and experiments were performed after 72-96 hours of post transduction.

Quantitative Reverse-Transcription Polymerase Chain Reaction (qRT-PCR): Total RNA was isolated from cultured cell using Trizol method (Life Technologies, Carlsbad, CA) as per manufacturers guidelines with some modification as described earlier (43). First strand cDNA was synthesized using the iScript Select cDNA Synthesis Kit and 1.0

297 μg of total RNA was used (Bio-Rad Laboratories, Hercules, CA) according to the
298 manufacturer's instructions. Quantitative real-time PCR was performed with iQ SYBR
299 Green super mix, using the iCycler iQ Real time PCR Detection System (Bio-Rad). Details
300 of the primers used for Myo1c, α-SMA and Col1α1 are described earlier (10, 44). Mouse
301 ribosomal protein S9 (RPS9) primer was used as a control to normalize the expression
302 (44).
303
304 **Western Blot Analysis**. Cultured cells were lysed in RIPA buffer and protein estimation
305 was performed using the BCA method. 20μg total protein samples from lysates were
306 used for western blotting analysis as described earlier (10). Mouse monoclonal Myo1c
307 antibody was used as reported earlier (10), whereas other antibodies, including GAPDH
308 (Sigma # G8795), α-SMA (Santa Cruz # c-53142) and Actin (Santa Cruz # sc-47778)
309 were commercially obtained. Western blotting image acquisition and densitometric
310 analysis was performed using LI-CORE imaging station as described earlier.
311
312 **Cell Migration Assay**: Cell migration assay was performed as described earlier with
313 some modification (45). Briefly, control and Myo1c knockdown GRX cells were grown in
314 35-mm glass-bottom culture dishes (Mat-Tek Corporation) until they reached confluence.
315 Scratches were created using a 200-μl sterile pipette tip and images were taken at 0h,
316 8h, 16h and 24h. ImageJ (National Institutes of Health) was used to calculate the length
317 of the wound's closure. The experiment was performed more than three times, and the
318 distance (μM) of migration was calculated.
319

Cell Proliferation Assay: Cell proliferation was determined using Cell Counting Kit-8 (CCK-8) as per manufacturer's instruction. Briefly, cells were plated in 96-well plates and incubated with CCK-8 solution for different time points such as 17 hours, 41 hours and 65 hours for GRX cells. Absorbance at 450 nm was measured using a microplate reader and extent of proliferation was measured. Cell proliferation was also determined using SRB Assay / Sulforhodamine B Assay Kit as per manufacturer's instruction. Briefly, in the assay, cultured GRX cells were fixed on plates and stained with Sulforhodamine B. Further, cells were washed and dried, then the bound dye was solubilized and the absorbance at 565 nm was measured.

Gel Contraction Assay: Contractility of control and Myo1c-KD GRX cells were evaluated using collagen gel lattices (PureCol, Advanced Biomatrix) as described earlier (46). Cells were cultured in 24-well culture plates in collagen gel lattice, where it was serum starved and after the dislodgement of the lattice, cells were incubated in DMEM with/without TGF-β1 (5 ng/mL) for 24 h. Collagen gel lattice size was determined at 0 hour as well as 24 hours post TGF-β treatment and area of gel contraction were calculated.

Treatments of animals: All experiments were performed in 8-12 weeks old mice. A Detailed experimental plan for animal treatment is given in **figure 5C** (19, 34). Wild-type and Myo1c-KO mice were treated with CCl4 (0.7ul/g body weight) or Vehicle (corn oil) through the intraperitoneal (i.p.) injection. Mice were randomly divided into 4 groups (n=5 for each group): **(1)** wild-type control group; treated with vehicle; **(2)** wild-type experimental group, treated with CCl4; **(3)** Myo1c-KO control group, treated with vehicles;

(4) Myo1c-KO experimental group, treated with CCl4. At 5th week of the treatment tissues were harvested for the experimental purpose.

Histology and Immunohistochemistry: Mice liver were perfused and washed with 1X PBS and transected, fixed for 4 to 12 h in 4% paraformaldehyde, rinsed, and sequential alcohol treatments were performed and submitted to the Histology Core facility at Medical University of South Carolina (MUSC) for embedding and sectioning. The paraffin embedded sections were deparaffinized and stained with Masson's trichrome and Sirius Red for histological analysis. Immunohistochemistry was performed as described earlier (10). Briefly, liver sections were deparaffinized and incubated with Tris-EDTA (pH 9.0) buffer for antigen retrieval at 65°C overnight. The sections then blocked with 5% BSA for 1 h at room temperature. Primary antibodies for α-SMA (1:50 dilution) were diluted in 10% goat serum and incubated overnight at 4°C. The sections were washed with 1× TBS five times and then incubated with Alexa Fluor-labeled secondary antibodies at a dilution of 1:500 for 1 h at 37°C. After washings with TBS these sections were mounted with DAPI and left overnight in the dark for drying and images were collected using fluorescence microscope. Horseradish peroxidase–conjugated anti-mouse or anti-rabbit antibodies were used for detection for non-fluorescence staining. All parameters were maintained constant throughout the image acquisition, including the exposure time. The image J software was used for quantitative analysis.

Human and Animal Study approval: De-identified, formalin fixed paraffin embedded liver tissue sections (n=5) from Dr. A Canbay (09-4252 & 12-5232-BO, Ethics

Commission, Medical Faculty of the University of Duisburg-Essen) were stained using established immunohistochemistry protocols. All animal studies were conducted as per the protocol approved by the MUSC, Institutional Animal Care and Use Committee and NIH guidelines for the Care and Use of Laboratory Animals (Protocol # IACUC-2018-00360). Treatment of mice, including housing, injections and surgery was in accordance with the institutional guidelines. Isoflurane anesthesia (5% induction, 2% maintenance) was used to perform all surgeries.

AUTHOR CONTRIBUTIONS

EA and WKS, conceptualization: EA, CW, AKS and BR, conducted the experiments and analyzed data. WKS, DN, JHL provided critical reagents and helped with experimental designs. EA and WKS designed the experiments, interpreted data, and wrote the manuscript. All authors discussed results and commented on the manuscript.

ACKNOWLEDGEMENTS

This study is supported by the Division of Gastroenterology and Hepatology, MUSC (W.K.S), the Ralph H Johnson Veterans Affairs Medical Center (W.K.S), and National Institutes of Health, NIDDK, Grant RO3 5R03TR003038-02 (E.A.).

CONFLICT OF INTEREST

The authors declare no conflict of interest.

FIGURE LEGENDS

Figure 1: Myo1c upregulated during fibrotic injury: (A) The GEO profile GDS3087 of Myo1c in hepatocellular tumors of Trim24 deficient mice was retrieved from GEO database and expression pattern of *Myo1c* was analyzed in normal liver vs hepatocellular tumors. Both, the expression level and rank of *Myo1c* were significantly increased in hepatocellular tumor as compared to normal liver. **(B)** GEO high throughput data (GEO # GSE49541), where mild NAFLD patients (with fibrosis stage 0-1) and advanced NAFLD (with fibrosis stage 3-4) were analyzed. We retrieve the data and Myo1c expression patterns were analyzed. Expression of Myo1c is found to be significantly upregulated in advanced NAFLD as compared to mild NAFLD. **(C-D)** Representative images of liver sections from NASH and normal subjects showed increased Myo1c expression in NASH. Images magnification, 10x (upper panel) and 40x (lower panel). Quantitative analysis of immunofluorescence images showed that Myo1c expression was elevated in NASH as compared to normal liver. P≤0.0001 NASH vs Normal. Data presented in mean±SD. **(E-F)** Representative images of liver sections from MCD-diet and normal chow diet showed increased Myo1c expression in MCD-diet mice. Images magnification, 10x (upper panel) and 40x (lower panel). Quantitative analysis of immunofluorescence images showed that Myo1c expression was elevated in MCD-diet liver as compared to normal chow-diet liver. P≤0.0001 MCD-diet vs Chow-diet. Data presented in mean±SD. **(G-H)** Representative images of liver sections from CCl4-induced mice model and control vehicle treated mice showed increased Myo1c expression in CCl4-induced mice. Images magnification, 10x (upper panel) and 40x (lower panel). Quantitative analysis of immunofluorescence images showed that Myo1c expression was elevated in CCl4-induced liver as compared

to normal vehicle treated liver section. P≤0.0001 MCD-diet vs Chow-diet. Data presented in mean±SD. **(I-J)** The hepatic stellate cells line (GRX) and mouse embryonic fibroblasts (MEFs) were treated with TGF-β for 48hours and expression of Myo1c was assessed by qPCR and normalized to ribosomal protein S9. Quantitative analysis showed the increased expression of Myo1c in both the cell lines upon TGF-β treatment. Data are from 3 independent experiments presented as mean±SD. TGF-β (-) *vs.* TGF-β (+); P≤0.01.

Figure 2: Myo1c deletion attenuates fibrogenic response: (A&B) Myo1c knockdown in GRX cell was induced by the lentiviral transfection of Myo1c shRNA, whereas scramble (SCR) transfection was done for controls. Stable transfection was achieved through the puromycin selection and the extent of the Myo1c protein knockdown was assessed by western blotting **(A)**, whereas qPCR **(B)** was performed to check knockdown at mRNA level. (C&D) To test the TGF-β induced activation then control and Myo1c knockdown GRX cells were investigated for the expression of the fibrogenic genes. TGF-β significantly upregulates the α-SMA **(C)** and Col1α1 **(D)** in control cells, whereas upregulation of these genes were blunted in Myo1c knockdown cells. **(E&F)** Effect of Myo1c inhibitor PCIP (0.1Mm) on TGF-β induced fibrogenic response was analyzed through the qPCR. PCIP treatment significantly blunted the α-SMA expression upon TGF-β, whereas, significant differences were observed in Col1α1 expression. Myo1c also contributes dysregulation of cell proliferation, abnormal wound healing and collagen gel contraction. Cell Counting Kit-8 (CCK-8) was used to measure cell proliferation in control and Myo1c knockdown GRX cells. **(G)** Absorbance at 450 nm, which a readout of the number of viable cells is significantly reduced upon Myo1c knockdown at 41 and 65 hours.

(H) Analysis of SRB based cell proliferation further confirmed that there is a significant reduction in cell proliferation in Myo1c knockdown cells. Data are from 3 independent experiments. The collagen gel contraction (CGC) assay was performed to analyze the fibrogenic response in presence TGF-β stimulation in GRX cells. **(3K&L)** TGF-β stimulation induced 54% of gel contraction in shScr-GRX (control) cells compared to 17% in shMyo1c-GRX.

Figure 3: (A) MEFs were isolated from Myo1c flox/flox mice and treated with either β-gal or Cre virus to generate control and Myo1c knockout MEFs, respectively. Western blotting analysis showed that Myo1c proteins were completely knockout after 96 hours of post viral treatment. **(B&C)** Control (Myo1cfl/fl-MEFs+βGal) and Myo1c-KO (Myo1cfl/fl-MEFs+Cre) MEFs were treated with TGF-β expression of α-SMA and Col1α1 genes were analyzed, where significant upregulation of these genes were observed in control MEFs but attenuated in Myo1c-KO MEFs. **(D)** TGF-β induced expression of α-SMA was analyzed through immunofluorescence staining, where cells MEFs were stained with α-SMA (Green) antibody and mounted with DAPI (Blue). **(E)** Quantitative analysis of fluorescence means pixel intensity showed increased expression of α-SMA in control MEFs as compared to Myo1c-KO MEFs (n = 50 cells). Data are from 3 independent experiments presented as mean±SD. SCR: scramble; N.S: non-significant. $p \leq 0.05$, Significant.

Figure 4: TGF-β induced signaling is blunted upon Myo1c inhibition and in Myo1c-deletion: (**A&B**) The signaling components of TGF-β signaling pathways in vehicle and

PCIP treated GRX cells were screened using western blotting. Quantitative analysis showed reduced phosphorylation of SMAD2 and SMAD3 expression in Myo1c-KO MEFs. Data are presented in mean±SD. (C-D) Similarly, the signaling components of TGF-β signaling pathways in control and Myo1c-KO MEFs were screened using western blotting. Quantitative analysis showed reduced phosphorylation of SMAD2 and SMAD3 expression in Myo1c-KO MEFs. Data are presented in mean±SD.

Figure 5: Myo1c deletion attenuates CCl4 induced liver fibrosis in mice: (A) Global Myo1c mice were generated using Myo1c flox/flox mice as presented in schematic figure. Myo1c flox/flox mice were crossed with CMV cre (B6.C-Tg(CMV-cre)1Cgn/J; Stock No: 006054), which eventually leads to deletion of the critical 5-13 exon of the Myo1c. **(B)** Deletion of Myo1c was confirmed through the western blotting analysis using specific Myo1c antibody, which showed complete knockout of Myo1c in liver and kidney. **(C)** Schematic figure showing experimental design including timelines of CCl4 treatment and end of the study. **(D)** Increased Masson's trichrome staining was noted in the liver of wild-type mice as compared to Myo1c-KO mice treated with CCl4. Scale bars: 50μm. **(E)** Fibrotic area assessment from the Masson's trichrome stained liver of wild-type mice showed ~8.2% fibrosis, whereas the Myo1c-KO showed ~3.37% fibrosis. $P \leq 0.001$, wild-type-CCl4 vs Myo1c-KO-CCl4, n=5 mice in each group using manual outlining method. Data presented in mean±SD**. (F)** Increased Sirius-red staining was also noted in the liver of wild-type mice as compared to Myo1c-KO mice treated with CCl4. Scale bars: 50μm. **(G)** Fibrotic area assessment from the Sirius-red stained liver of wild-type mice showed ~9.7% fibrosis, whereas the Myo1c-KO showed ~5.7% fibrosis. $P \leq 0.001$, wild-type-CCl4

vs Myo1c-KO-CCl4, n=5 mice in each group using manual outlining method. Data presented in mean±SD**.**

Figure 6: (A) Immunostaining of liver sections using α-SMA antibody and DAPI (blue) showed increased α-SMA expression in wild-type mice in response to CCl4 induced injury. Scale bars: 20μm **(B)** Quantitative analysis of immunofluorescence images showed that CCl4 injury-induced α-SMA expression was elevated in wild-type mice when compared to Myo1c-KO mice. P≤0.01 wild-type (CCl4) vs Myo1c-KO (CCl4). n=5 mice in each group. Data presented in mean±SD. **(C)** Immunostaining of liver sections using α-SMA antibody and HRP conjugated secondary antibody showed increased α-SMA positive area in wild-type mice in response to CCl4 induced injury. (upper panel 10x; lower panel 40x magnification) **(D)** Quantitative analysis of α-SMA positive area showed that CCl4 injury-induced significant increase in α-SMA positive area in wild-type mice when compared to Myo1c-KO mice. Data presented in mean±SD.

Supplemental Figure 1: (A&B) Upregulation of Myo1c in CCl4 induced liver injury was further confirmed through the western blotting. Quantitative analysis showed the increased expression of Myo1c in CCl4 induced liver as compared to vehicle treated. P<0.04, CCl4 induced liver injury vs vehicle treated controls. Data presented in mean±SD. **(C&D)** The expression analysis of *Myo1c* and *α-SMA* in HFD and LFD mice liver were analyzed using qPCR. Expression of Myo1c was significantly upregulated in the HFD liver compared to LFD. Data are from 3 independent experiments presented as mean±SD. HFD *vs.* LFD; P≤0.05.

REFERENCES

1. Yi, H.S., et al., *Treatment with 4-methylpyrazole modulated stellate cells and natural killer cells and ameliorated liver fibrosis in mice.* PLoS One, 2015. **10**(5): p. e0127946.
2. Tanaka, M. and A. Miyajima, *Liver regeneration and fibrosis after inflammation.* Inflamm Regen, 2016. **36**: p. 19.
3. Bataller, R. and D.A. Brenner, *Liver fibrosis.* J Clin Invest, 2005. **115**(2): p. 209-18.
4. Eghbali-Fatourechi, G., et al., *Type I procollagen production and cell proliferation is mediated by transforming growth factor-beta in a model of hepatic fibrosis.* Endocrinology, 1996. **137**(5): p. 1894-903.
5. Gressner, A.M. and R. Weiskirchen, *Modern pathogenetic concepts of liver fibrosis suggest stellate cells and TGF-beta as major players and therapeutic targets.* J Cell Mol Med, 2006. **10**(1): p. 76-99.
6. Lu, N., et al., *Hepatocyte-specific ablation of PP2A catalytic subunit alpha attenuates liver fibrosis progression via TGF-beta1/Smad signaling.* Biomed Res Int, 2015. **2015**: p. 794862.
7. Chung, C.L., et al., *Pentachloropseudilin Inhibits Transforming Growth Factor-beta (TGF-beta) Activity by Accelerating Cell-Surface Type II TGF-beta Receptor Turnover in Target Cells.* Chembiochem, 2018. **19**(8): p. 851-864.
8. Capmany, A., et al., *MYO1C stabilizes actin and facilitates the arrival of transport carriers at the Golgi complex.* J Cell Sci, 2019. **132**(8).
9. Venit, T., et al., *Nuclear myosin I regulates cell membrane tension.* Sci Rep, 2016. **6**: p. 30864.
10. Arif, E., et al., *The motor protein Myo1c regulates transforming growth factor-beta-signaling and fibrosis in podocytes.* Kidney Int, 2019. **96**(1): p. 139-158.
11. Fan, Y., et al., *Myo1c facilitates G-actin transport to the leading edge of migrating endothelial cells.* J Cell Biol, 2012. **198**(1): p. 47-55.
12. Venit, T., et al., *Mouse nuclear myosin I knock-out shows interchangeability and redundancy of myosin isoforms in the cell nucleus.* PLoS One, 2013. **8**(4): p. e61406.
13. Philimonenko, V.V., et al., *Nuclear actin and myosin I are required for RNA polymerase I transcription.* Nat Cell Biol, 2004. **6**(12): p. 1165-72.
14. Zattelman, L., et al., *N-terminal splicing extensions of the human MYO1C gene fine-tune the kinetics of the three full-length myosin IC isoforms.* J Biol Chem, 2017. **292**(43): p. 17804-17818.
15. Khetchoumian, K., et al., *Loss of Trim24 (Tif1alpha) gene function confers oncogenic activity to retinoic acid receptor alpha.* Nat Genet, 2007. **39**(12): p. 1500-6.
16. Jiang, S., et al., *TRIM24 suppresses development of spontaneous hepatic lipid accumulation and hepatocellular carcinoma in mice.* J Hepatol, 2015. **62**(2): p. 371-9.
17. Moylan, C.A., et al., *Hepatic gene expression profiles differentiate presymptomatic patients with mild versus severe nonalcoholic fatty liver disease.* Hepatology, 2014. **59**(2): p. 471-82.
18. Machado, M.V., et al., *Mouse models of diet-induced nonalcoholic steatohepatitis reproduce the heterogeneity of the human disease.* PLoS One, 2015. **10**(5): p. e0127991.
19. Dai, C., et al., *Chloroquine ameliorates carbon tetrachloride-induced acute liver injury in mice via the concomitant inhibition of inflammation and induction of apoptosis.* Cell Death Dis, 2018. **9**(12): p. 1164.
20. Chen, H.J. and J. Liu, *Actein ameliorates hepatic steatosis and fibrosis in high fat diet-induced NAFLD by regulation of insulin and leptin resistant.* Biomed Pharmacother, 2018. **97**: p. 1386-1396.
21. Herrmann, J., A.M. Gressner, and R. Weiskirchen, *Immortal hepatic stellate cell lines: useful tools to study hepatic stellate cell biology and function?* J Cell Mol Med, 2007. **11**(4): p. 704-22.
22. Mori, Y., et al., *Connective tissue growth factor/CCN2-null mouse embryonic fibroblasts retain intact transforming growth factor-beta responsiveness.* Exp Cell Res, 2008. **314**(5): p. 1094-104.

23. Lombardi, A.A., et al., *Mitochondrial calcium exchange links metabolism with the epigenome to control cellular differentiation.* Nat Commun, 2019. **10**(1): p. 4509.
24. Tang, L.Y., et al., *Transforming Growth Factor-beta (TGF-beta) Directly Activates the JAK1-STAT3 Axis to Induce Hepatic Fibrosis in Coordination with the SMAD Pathway.* J Biol Chem, 2017. **292**(10): p. 4302-4312.
25. Higashi, T., S.L. Friedman, and Y. Hoshida, *Hepatic stellate cells as key target in liver fibrosis.* Adv Drug Deliv Rev, 2017. **121**: p. 27-42.
26. Toyama, T., et al., *Noncanonical Wnt11 inhibits hepatocellular carcinoma cell proliferation and migration.* Mol Cancer Res, 2010. **8**(2): p. 254-65.
27. Brandstaetter, H., et al., *Loss of functional MYO1C/myosin 1c, a motor protein involved in lipid raft trafficking, disrupts autophagosome-lysosome fusion.* Autophagy, 2014. **10**(12): p. 2310-23.
28. Xue, M. and C.J. Jackson, *Extracellular Matrix Reorganization During Wound Healing and Its Impact on Abnormal Scarring.* Adv Wound Care (New Rochelle), 2015. **4**(3): p. 119-136.
29. Rockey, D.C., et al., *Smooth Muscle alpha-Actin Deficiency Leads to Decreased Liver Fibrosis via Impaired Cytoskeletal Signaling in Hepatic Stellate Cells.* Am J Pathol, 2019. **189**(11): p. 2209-2220.
30. Gonzalez-Andrades, M., et al., *Establishment of a novel in vitro model of stratified epithelial wound healing with barrier function.* Sci Rep, 2016. **6**: p. 19395.
31. Vernon, R.B. and M.D. Gooden, *An improved method for the collagen gel contraction assay.* In Vitro Cell Dev Biol Anim, 2002. **38**(2): p. 97-101.
32. Kobayashi, T., et al., *TGF-beta1 and serum both stimulate contraction but differentially affect apoptosis in 3D collagen gels.* Respir Res, 2005. **6**: p. 141.
33. Chinthalapudi, K., et al., *Mechanism and specificity of pentachloropseudilin-mediated inhibition of myosin motor activity.* J Biol Chem, 2011. **286**(34): p. 29700-8.
34. Ma, X., et al., *Androgen aggravates liver fibrosis by activation of NLRP3 inflammasome in CCl4-induced liver injury mouse model.* Am J Physiol Endocrinol Metab, 2020. **318**(5): p. E817-E829.
35. Greenwel, P., et al., *Characterization of fat-storing cell lines derived from normal and CCl4-cirrhotic livers. Differences in the production of interleukin-6.* Lab Invest, 1991. **65**(6): p. 644-53.
36. Carpino, G., et al., *Alpha-SMA expression in hepatic stellate cells and quantitative analysis of hepatic fibrosis in cirrhosis and in recurrent chronic hepatitis after liver transplantation.* Dig Liver Dis, 2005. **37**(5): p. 349-56.
37. Bose, A., et al., *Glucose transporter recycling in response to insulin is facilitated by myosin Myo1c.* Nature, 2002. **420**(6917): p. 821-4.
38. Hou, W. and W.K. Syn, *Role of Metabolism in Hepatic Stellate Cell Activation and Fibrogenesis.* Front Cell Dev Biol, 2018. **6**: p. 150.
39. Tiwari, A., et al., *The myosin motor Myo1c is required for VEGFR2 delivery to the cell surface and for angiogenic signaling.* Am J Physiol Heart Circ Physiol, 2013. **304**(5): p. H687-96.
40. Arif, E., et al., *Structural Analysis of the Myo1c and Neph1 Complex Provides Insight into the Intracellular Movement of Neph1.* Mol Cell Biol, 2016. **36**(11): p. 1639-54.
41. Takenouchi, Y., et al., *Growth differentiation factor 15 facilitates lung fibrosis by activating macrophages and fibroblasts.* Exp Cell Res, 2020. **391**(2): p. 112010.
42. Syn, W.K., et al., *Hedgehog-mediated epithelial-to-mesenchymal transition and fibrogenic repair in nonalcoholic fatty liver disease.* Gastroenterology, 2009. **137**(4): p. 1478-1488 e8.
43. Arffa, M.L., et al., *Epigallocatechin-3-Gallate Upregulates miR-221 to Inhibit Osteopontin-Dependent Hepatic Fibrosis.* PLoS One, 2016. **11**(12): p. e0167435.
44. Choi, S.S., et al., *Leptin promotes the myofibroblastic phenotype in hepatic stellate cells by activating the hedgehog pathway.* J Biol Chem, 2010. **285**(47): p. 36551-60.
45. Omenetti, A., et al., *Repair-related activation of hedgehog signaling promotes cholangiocyte chemokine production.* Hepatology, 2009. **50**(2): p. 518-27.

600 46. Rockey, D.C., C.N. Housset, and S.L. Friedman, *Activation-dependent contractility of rat hepatic*
601 *lipocytes in culture and in vivo.* J Clin Invest, 1993. **92**(4): p. 1795-804.

602

Figure 1

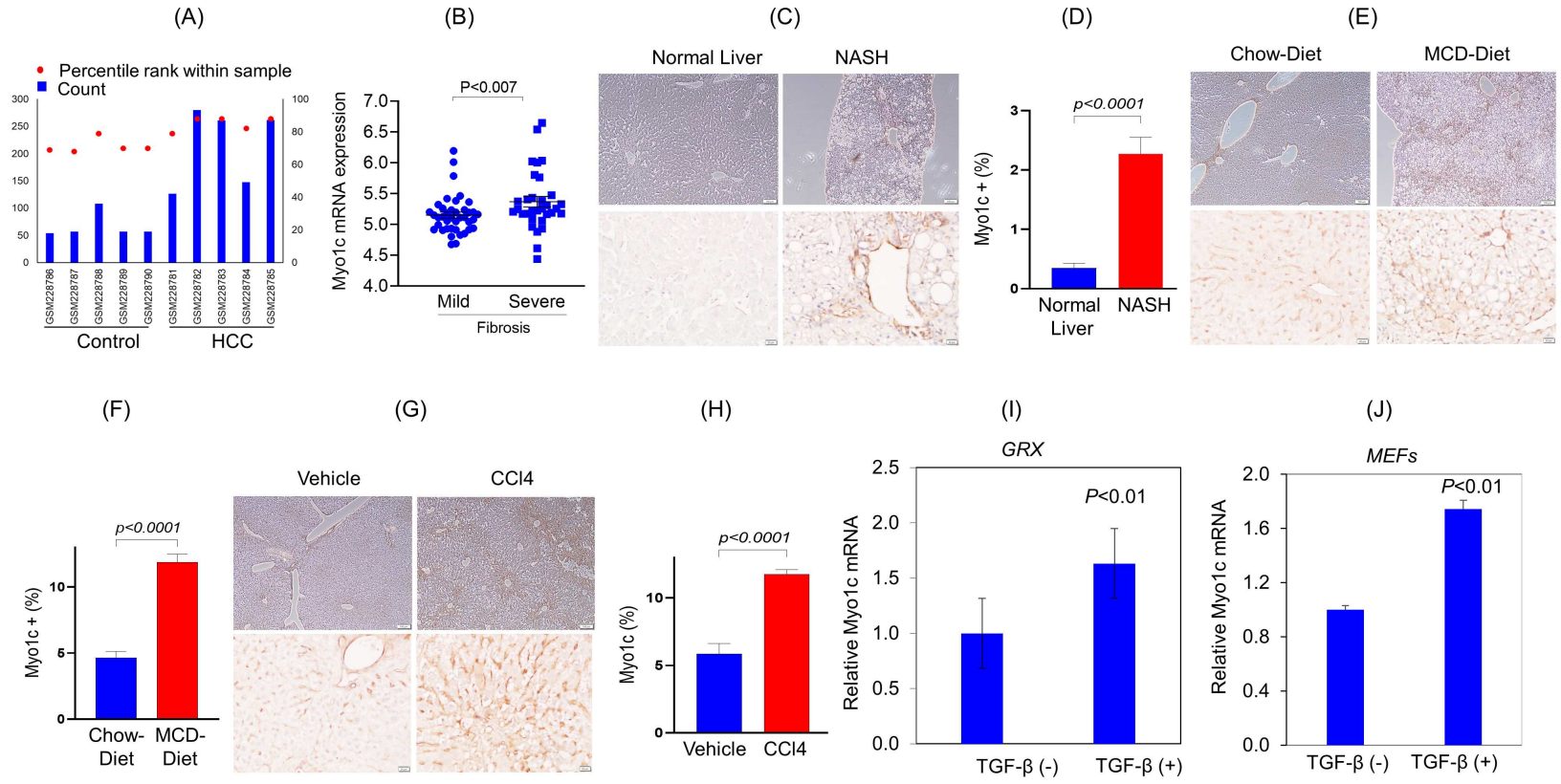
(A)
Percentile rank within sample
Count
GSM228786
GSM228787
GSM228788
GSM228789
GSM228790
GSM228781
GSM228782
GSM228783
GSM228784
GSM228785
Control
HCC
(B)
P<0.007
Myo1c mRNA expression
Mild
Severe
Fibrosis
(C)
Normal Liver
NASH
(D)
p<0.0001
Myo1c + (%)
Normal Liver
NASH
(E)
Chow-Diet
MCD-Diet
(F)
p<0.0001
Myo1c + (%)
Chow-Diet
MCD-Diet
(G)
Vehicle
CCl4
(H)
p<0.0001
Myo1c (%)
Vehicle
CCl4
(I)
GRX
P<0.01
Relative Myo1c mRNA
TGF-β (-)
TGF-β (+)
(J)
MEFs
P<0.01
Relative Myo1c mRNA
TGF-β (-)
TGF-β (+)

Figure 2

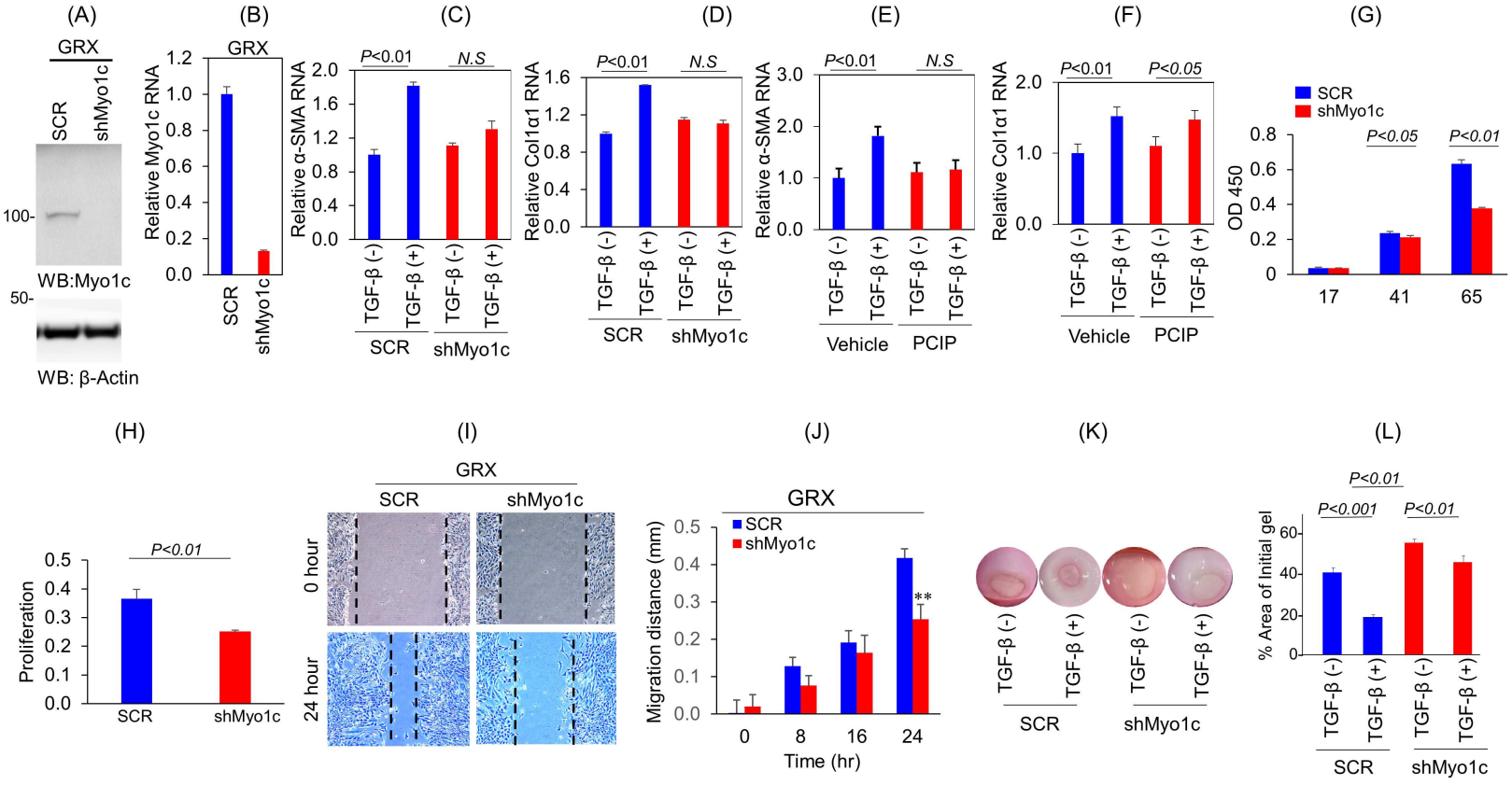
(A)
GRX
SCR
shMyo1c
100-
WB:Myo1c
50-
WB: β-Actin
(B)
GRX
Relative Myo1c RNA
SCR
shMyo1c
(C)
P<0.01
N.S
Relative α-SMA RNA
TGF-β (-)
TGF-β (+)
SCR
shMyo1c
(D)
P<0.01
N.S
Relative Col1α1 RNA
SCR
shMyo1c
(E)
P<0.01
N.S
Relative α-SMA RNA
Vehicle
PCIP
(F)
P<0.01
P<0.05
Relative Col1α1 RNA
Vehicle
PCIP
(G)
SCR
shMyo1c
P<0.05
P<0.01
OD 450
17
41
65
(H)
P<0.01
Proliferation
SCR
shMyo1c
(I)
GRX
SCR
shMyo1c
0 hour
24 hour
(J)
GRX
SCR
shMyo1c
Migration distance (mm)
**
Time (hr)
(K)
TGF-β (-)
TGF-β (+)
SCR
shMyo1c
(L)
P<0.01
P<0.001
P<0.01
% Area of Initial gel
TGF-β (-)
TGF-β (+)
SCR
shMyo1c

Figure 3

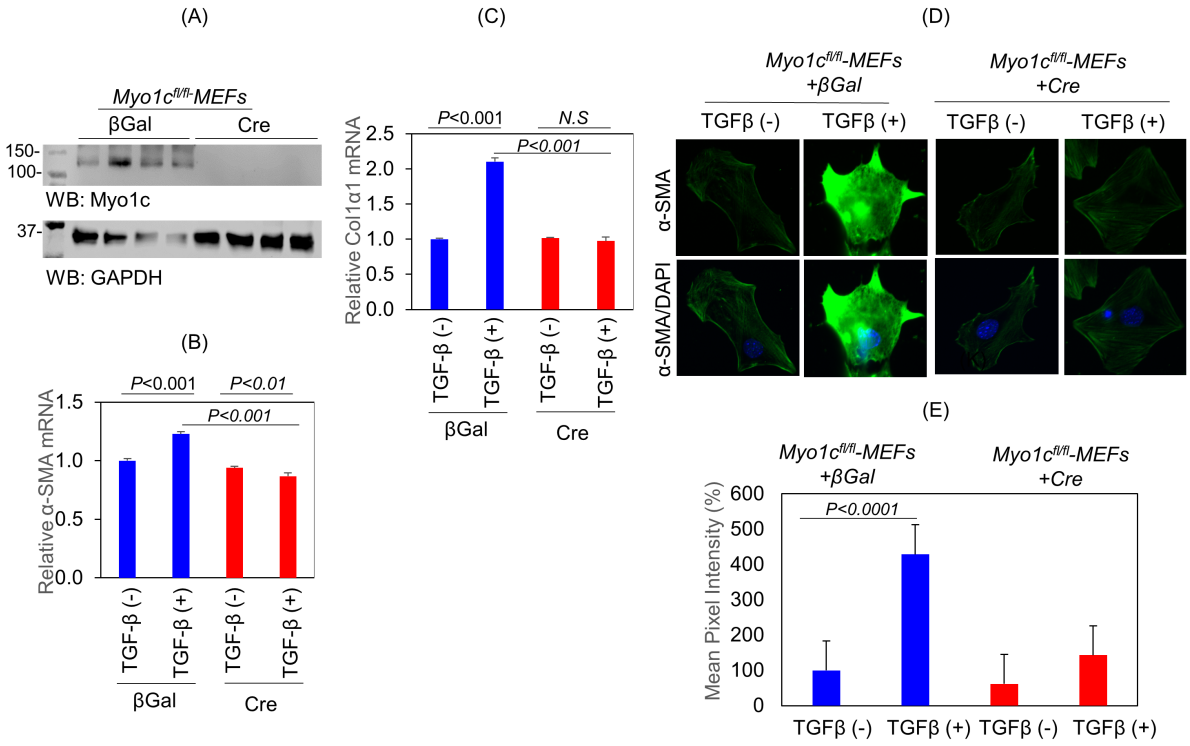
(A)
Myo1c^fl/fl-MEFs
βGal
Cre
150-
100-
WB: Myo1c
37-
WB: GAPDH
(B)
Relative α-SMA mRNA
P<0.001
P<0.01
P<0.001
TGF-β (-)
TGF-β (+)
TGF-β (-)
TGF-β (+)
βGal
Cre
(C)
Relative Col1α1 mRNA
P<0.001
N.S
P<0.001
(D)
Myo1c^fl/fl-MEFs +βGal
Myo1c^fl/fl-MEFs +Cre
TGFβ (-)
TGFβ (+)
α-SMA
α-SMA/DAPI
(E)
Mean Pixel Intensity (%)
P<0.0001

Figure 4

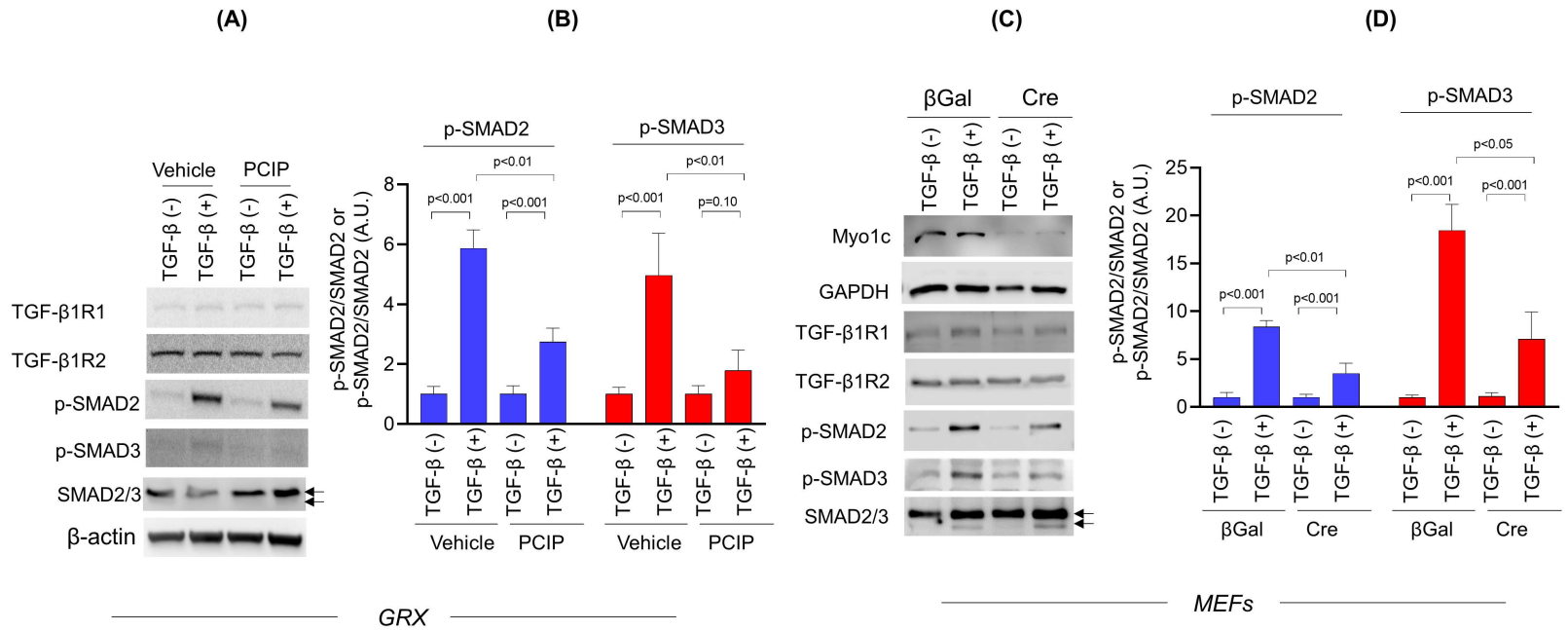
(A)
(B)
(C)
(D)
Vehicle
PCIP
TGF-β (-)
TGF-β (+)
TGF-β1R1
TGF-β1R2
p-SMAD2
p-SMAD3
SMAD2/3
β-actin
p-SMAD2
p-SMAD3
p-SMAD2/SMAD2 or p-SMAD2/SMAD2 (A.U.)
p<0.001
p<0.01
p=0.10
βGal
Cre
Myo1c
GAPDH
p<0.05
GRX
MEFs

Figure 5

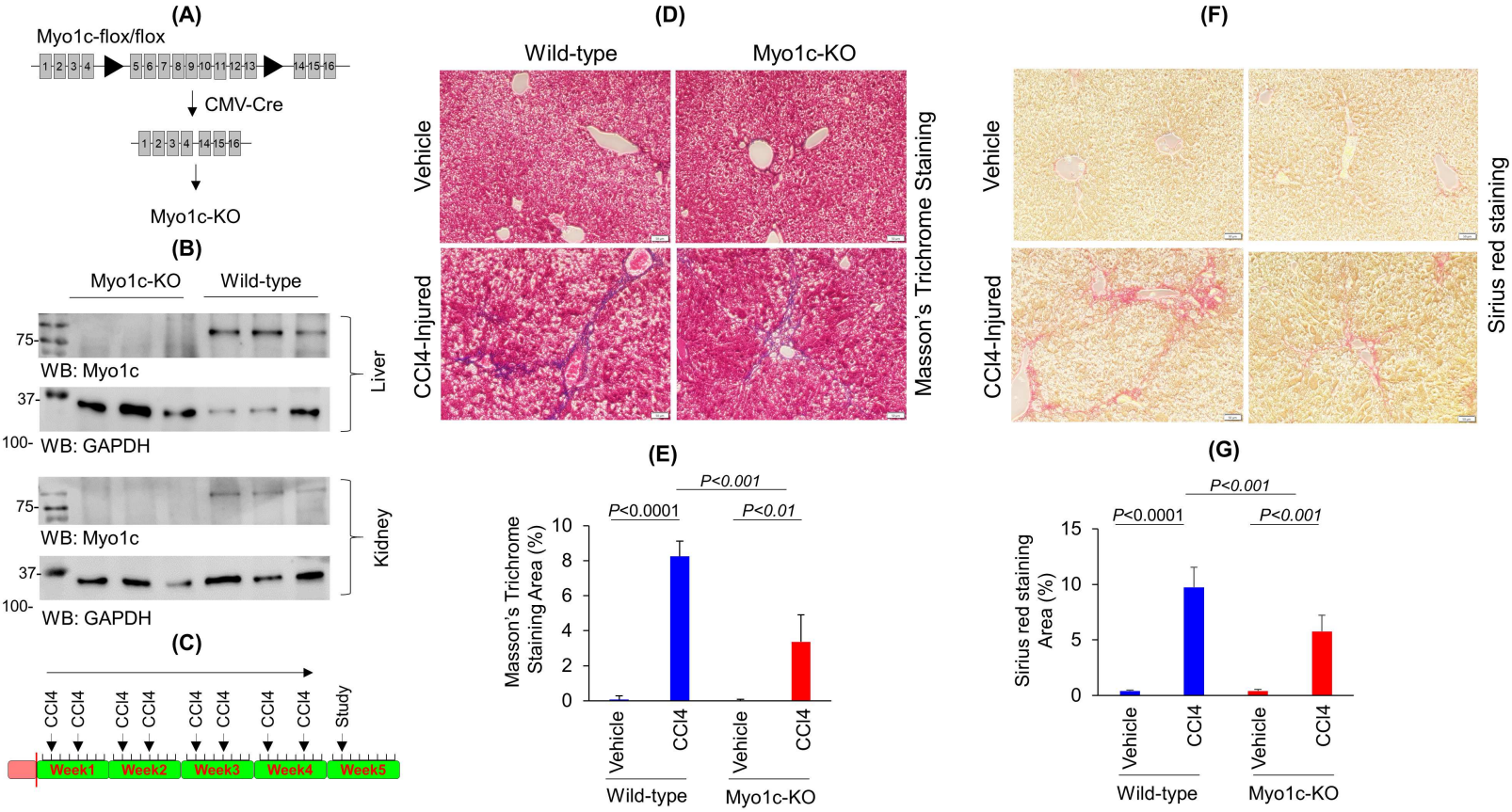
(A)
Myo1c-flox/flox
1 2 3 4 5 6 7 8 9 10 11 12 13 14 15 16
CMV-Cre
1 2 3 4 14 15 16
Myo1c-KO
(B)
Myo1c-KO
Wild-type
75-
WB: Myo1c
37-
100-
WB: GAPDH
Liver
75-
WB: Myo1c
37-
100-
WB: GAPDH
Kidney
(C)
CCl4
CCl4
CCl4
CCl4
CCl4
CCl4
CCl4
CCl4
Study
Week1
Week2
Week3
Week4
Week5
(D)
Wild-type
Myo1c-KO
Vehicle
CCl4-Injured
Masson's Trichrome Staining
(E)
P<0.001
P<0.0001
P<0.01
Masson's Trichrome Staining Area (%)
0
2
4
6
8
10
Vehicle
CCl4
Vehicle
CCl4
Wild-type
Myo1c-KO
(F)
Vehicle
CCl4-Injured
Sirius red staining
(G)
P<0.001
P<0.0001
P<0.001
Sirius red staining Area (%)
0
5
10
15
Vehicle
CCl4
Vehicle
CCl4
Wild-type
Myo1c-KO

Figure 6

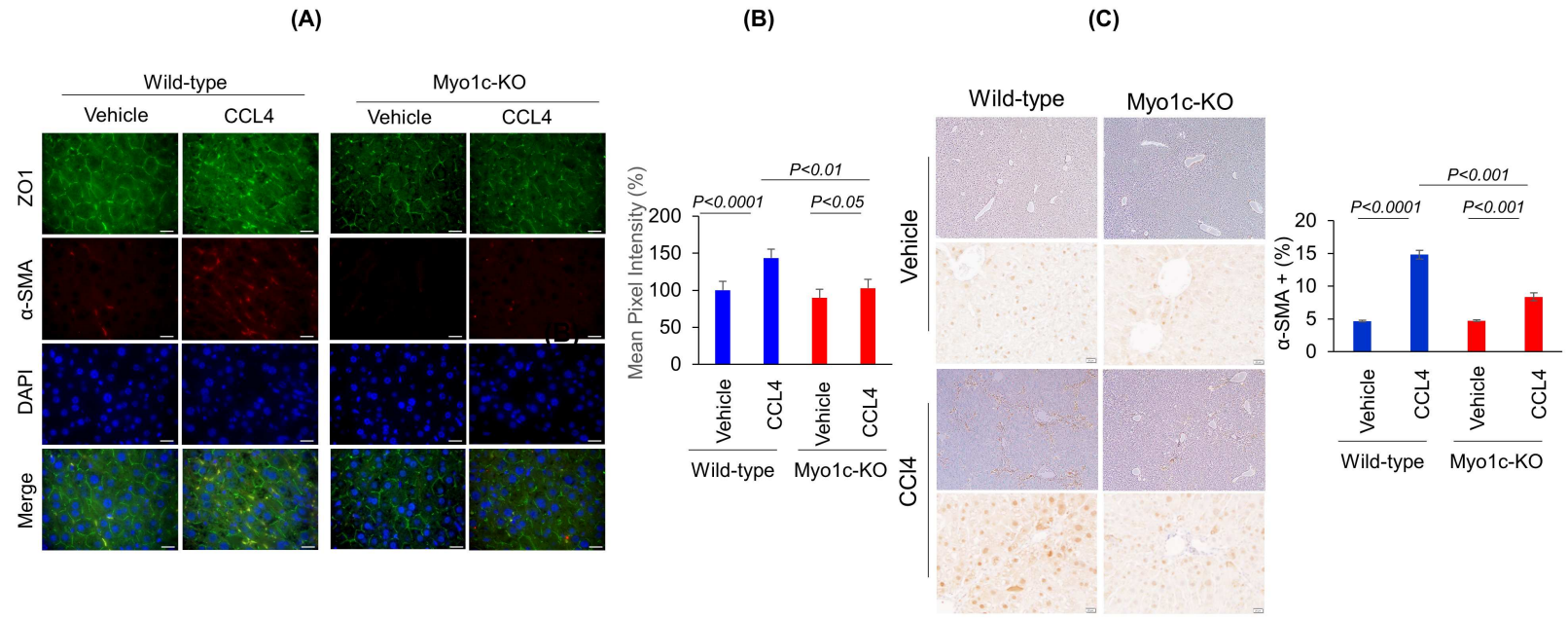
(A)
(B)
(C)
Wild-type
Myo1c-KO
Vehicle
CCL4
ZO1
α-SMA
DAPI
Merge
Mean Pixel Intensity (%)
P<0.0001
P<0.05
P<0.01
Wild-type
Myo1c-KO
CCl4
α-SMA + (%)
P<0.0001
P<0.001
P<0.001

Supplemental Figure 1

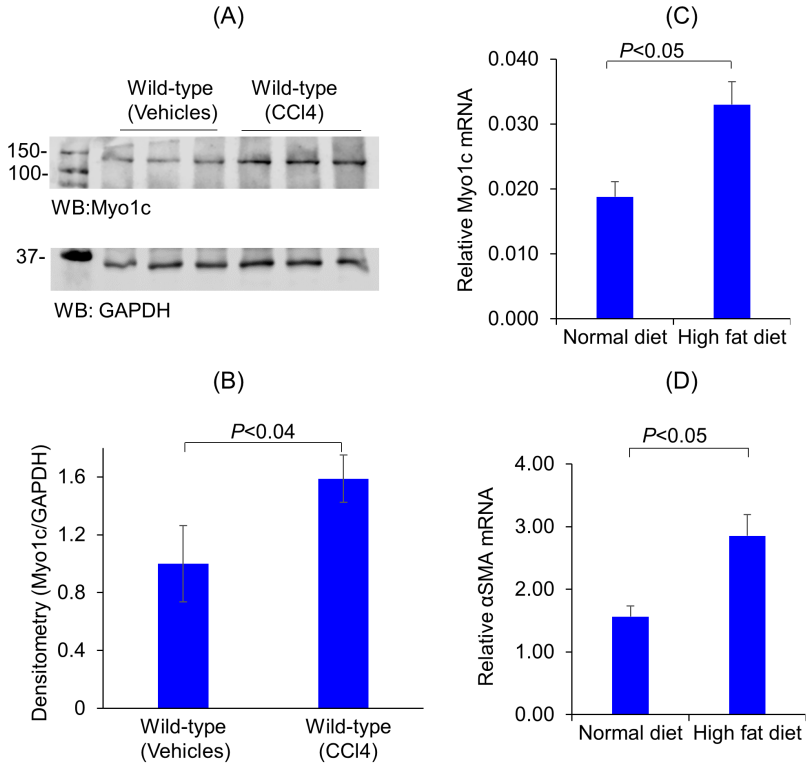

Abstract

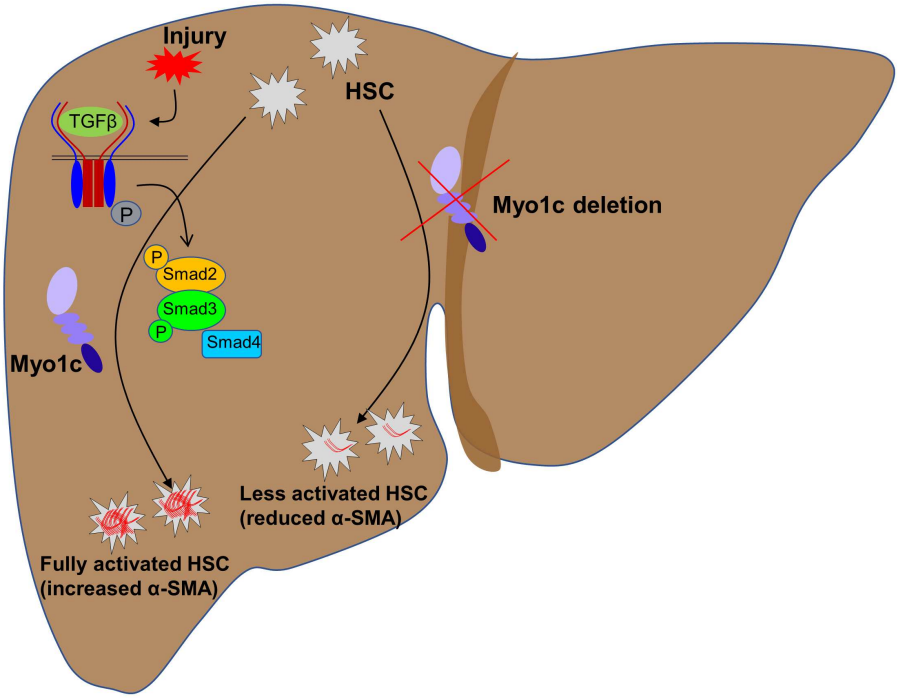
Injury
HSC
TGFβ
P
Myo1c deletion
P
Smad2
Smad3
P
Smad4
Myo1c
Less activated HSC
(reduced α-SMA)
Fully activated HSC
(increased α-SMA)